Icarus 300 (2018) 167–173

Contents lists available at ScienceDirect

Icarus

journal homepage: www.elsevier.com/locate/icarus

Derivation of optical constants for nanophase hematite and application to modeled abundances from in-situ Martian reflectance spectra

Paul G. Lucey[a], David Trang[a,*], Jeffrey R. Johnson[b], Timothy D. Glotch[c]

[a] University of Hawai'i at Mānoa, Hawai'i Institute of Geophysics and Planetology, Honolulu, HI, 96822, USA
[b] Johns Hopkins University, Applied Physics Laboratory, Laurel, MD 20723, USA
[c] Department of Geological Sciences, Stony Brook University, Stony Brook, NY 11794, USA

ARTICLE INFO

Article history:
Received 10 May 2017
Revised 5 September 2017
Accepted 7 September 2017
Available online 9 September 2017

Keywords:
Mars spectroscopy
Mars
Mars mineralogy

ABSTRACT

Several studies have detected the presence of nanophase ferric oxide, such as nanophase hematite, across the martian surface through spacecraft and rover data. In this study, we used the radiative transfer method to detect and quantify the abundance of these nanophase particles. Because the visible/near-infrared spectral characteristics of hematite > 10 nm in size are different from nanophase hematite < 10 nm, there are not any adequate optical constants of nanophase hematite to study visible to near-infrared rover/spacecraft data of the martian surface. Consequently, we found that radiative transfer models based upon the optical constants of crystalline hematite are unable to reproduce laboratory spectra of nanophase hematite. In order to match the model spectra to the laboratory spectra, we developed a new set of optical constants of nanophase hematite in the visible and near-infrared and found that radiative transfer models based upon these optical constants consistently model the laboratory spectra. We applied our model to the passive bidirectional reflectance spectra data from the Chemistry and Camera (ChemCam) instrument onboard the Mars Science Laboratory rover, Curiosity. After modeling six spectra representing different major units identified during the first year of rover operations, we found that the nanophase hematite abundance was no more than 4 wt%.

1. Introduction

1.1. The spectra of nanophase hematite

The red color of Mars has long been known to be due to the presence of ferric oxide, but with few exceptions the reflectance spectrum of Mars is inconsistent with the presence of crystalline ferric oxides. Ferric iron-bearing minerals typically exhibit a spectral shoulder near 700 nm and an absorption feature near 860 nm. However, in most spectra of Mars, this 860 nm absorption feature is absent (Singer et al., 1979; Bell et al., 2004). Analyses of in-situ data showed that nanophase ferric oxide particles, such as nanophase hematite, are ubiquitous on Mars. Various data sets (i.e., Mössbauer Spectrometer, Panoramic Camera, Alpha Proton X-ray Spectrometer) from the Spirit and Opportunity Mars Exploration Rovers showed evidence of nanophase ferric oxide at Meridiani Planum and Gusev Crater (Bell et al., 2004; Yen et al., 2005; Morris et al. 2006).

Morris et al. (1989) showed that nanophase particles of hematite are the likely coloring agent of Mars. They prepared samples with nanophase hematite with grain sizes < 10 nm suspended in silica and alumina matrices and found that the spectra do not exhibit the 860 nm absorption feature, unlike the spectra of bulk hematite. Based upon analysis of Mössbauer spectra, Morris et al. (1989) found that when nanophase hematite particles are > 10 nm, their visible to near-infrared spectra showed very distinct crystalline hematite bands reminiscent of spectra of pure bulk hematite powders. Morris et al. (1989) hypothesized that the absence of the 860 nm absorption in samples containing < 10 nm sized hematite particles was due to the compromised crystalline structure of hematite at these small sizes. In all hematite particles, the surface and near surface of a particle do not have a well-formed hematite crystalline structure resulting in a poorly defined ligand field, preventing the development of the 860 nm absorption feature. On the other hand, the core of a particle has a well-defined crystalline structure leading to a strong ligand field that produces the 860 nm absorption feature. In large hematite particles (> 10 nm), the ratio of core volume, which contains well-defined crystalline structure, to surface volume, which contains poorly defined crystalline structure, is high, resulting in spectra of these particles exhibiting the 860 nm absorption feature. Because

* Corresponding author.
E-mail addresses: lucey@higp.hawaii.edu, dtrang@hawaii.edu (D. Trang).

http://dx.doi.org/10.1016/j.icarus.2017.09.010
0019-1035/

small hematite particles with sizes < 10 nm have low core to surface volume, the 860 nm absorption feature is largely absent in the spectra of these particles.

An alternative hypothesis for the spectral differences between samples containing large and small nanophase particles (e.g., presence of the 860 nm feature) is the unusual scattering properties at the finest scale (e.g., Steyer, 1974; Marra et al., 2011). Hapke (2001) presented a formulation to model the optical effect of nanophase particles in a transparent matrix, while Lucey and Noble (2008) showed that the Hapke (2001) model successfully reproduced spectra of experimentally produced nanophase native iron (Fe^0) within a silica host. However, the optical properties of native iron vary smoothly with wavelength, while hematite varies strongly, so the effects demonstrated numerically (Hapke, 2001) and experimentally (Noble et al., 2007) are not directly informative of the scattering influence on spectra of materials containing nanophase hematite. Nevertheless, the effect of size of nanophase particles on spectra of transparent hosts infused with this coloring agent is strong, so the optical effect of the nanophase size merits investigation.

In this paper we used the Hapke (2001) model and investigated its ability to reproduce the spectra of Morris et al. (1989) nanophase hematite particles, including modifications necessary to improve performance. We then applied our radiative transfer model to representative passive reflectance spectra obtained by the Chemistry and Camera (ChemCam) instrument during the first year of Curiosity Rover operations to estimate the nanophase hematite abundance near the landing site within Gale crater.

1.2. Radiative transfer model of nanophase particle spectra

Hapke (2001) developed a radiative transfer model to account for the strong optical effects associated with space weathering on airless objects within the inner solar system. Hapke (2001) attributed at least some of these effects to be due to tens of nanometer-sized native iron particles detected in lunar soils by ferromagnetic resonance techniques (Morris, 1976; 1978). Such particles were directly imaged by Keller and McKay (1997) and found to reside in rims on grains within lunar soils. Hapke (2001) presented a simple spectral model that to first order displayed the darkening and reddening of the visible to near-infrared reflectance associated with space weathering.

Lucey and Noble (2008) applied the Hapke (2001) model to visible and near-infrared spectra of a series of samples prepared by Noble et al. (2007) of porous silica matrices infused with nanophase native iron particles. The iron-bearing silica gels were ground and sieved to fixed size ranges followed by spectral measurements of each sample. The sample preparation methodology that they employed was that of Morris et al. (1989) with an additional step to reduce the ferric iron to native iron. These simple samples exhibited similar spectral properties found in nanophase native iron-bearing lunar soils, in which with increasing nanophase native iron abundance the samples displayed increasingly darkened and reddened reflectance spectra. Lucey and Noble (2008) found that for the sample series containing the smallest of the native iron particles (< 50 nm), Hapke's (2001) model was successful both at producing spectra that mimicked the empirical data and predicting the nanophase native iron abundance.

We will be applying the Hapke (2001) technique to hematite to determine if it can reproduce fine-grained hematite spectra. To do this, we need to find a suitable set of hematite optical constants. There are several hematite optical constants throughout the literature (e.g., Popova et al., 1973; Onari et al., 1977; Querry, 1985), but differ in spectral range and resolution. In addition several optical constants derivations are based on bulk hematite (Steyer, 1974; Onari et al., 1977; Bedidi and Cerville, 1993; Glotch et al., 2006; Marra et al., 2005; 2011) or fine-grained hematite (Kerker et al., 1979; Gillespie and Lindberg, 1992), which include spectral coverage of the visible to mid infrared wavelengths. Similar to the findings by Morris et al. (1989), several previous optical constants studies were unable to use bulk hematite optical constants to match the spectra of fine-grained hematite (Steyer, 1974; Marra et al., 2011). In this work, we will use the Querry (1985) optical constants because it covers the same spectral range as the laboratory spectra in Morris et al. (1989) with high spectral resolution. Therefore, this work would provide a new set of nanophase hematite optical constants in the visible and into the near infrared, which contains important absorptions in these wavelengths to study Martian mineralogy, and would be able to properly match fine-grained hematite spectra.

We use the Hapke (2001) approach in this work because it provided a validated model to the study of absorbing nanophase particles in a transparent silicate matrix; the Hapke (2001) model is well suited to quantitatively reproduce the spectral effects of nanophase hematite (< 10 nm in grain size) in silica gel as prepared and observed by Morris et al. (1989). Nanophase hematite is an interesting case from a modeling standpoint because the absorption of native iron is high throughout the visible and near infrared, but the spectra of hematite shows strong absorptions at short wavelengths (i.e., imaginary index of refraction values of ~1 near 400 nm), relatively low absorptions at near-infrared wavelengths, and a strong decrease in absorption between 400 and 600 nm.

Table 1
Sample names with their associated ferric oxide abundance.

Sample	Fe_2O_3 [wt%]
S6BLANK	0.0
S6FN14	0.2
S6FN3	0.3
S6FN18	0.5
S5FN29	0.7
S6FN1	1.3
S6FN4	3.4
S6FN10	5.2
S6FN10	5.2
S6FN11	6.0
S6FN24	8.3
S6FN28	11.0
S6FN27	16.7

2. Methods

For this work, we used reflectance spectra of the Morris et al. (1989) "Type D" samples that were shown by analysis of Mössbauer spectra to contain only hematite particles with sizes < 10.2 nm (Fig. 1a). The weight fraction of hematite particles within the samples ranged between 0 and 17 wt% (Table 1). The silica gel host particles ranged in size from 35–74 μm in size. With the exception of an iron-free sample (i.e., S6BLANK), the spectra of the samples feature properties reminiscent of those of Mars, such as the strong drop off in reflectance toward the blue portion of the spectrum and the absence of crystalline hematite features that are only occasionally observed in martian spectra (e.g., McCord et al., 1977).

We modeled the Morris et al. (1989) sample spectra using the Hapke (2001) radiative transfer model that includes the Maxwell–Garnett method to model visible to near-infrared spectra of powdered material that are coated with particles smaller than the wavelength of light (e.g., nanophase particles). Therefore, this radiative transfer model is applicable to the Morris et al. (1989)

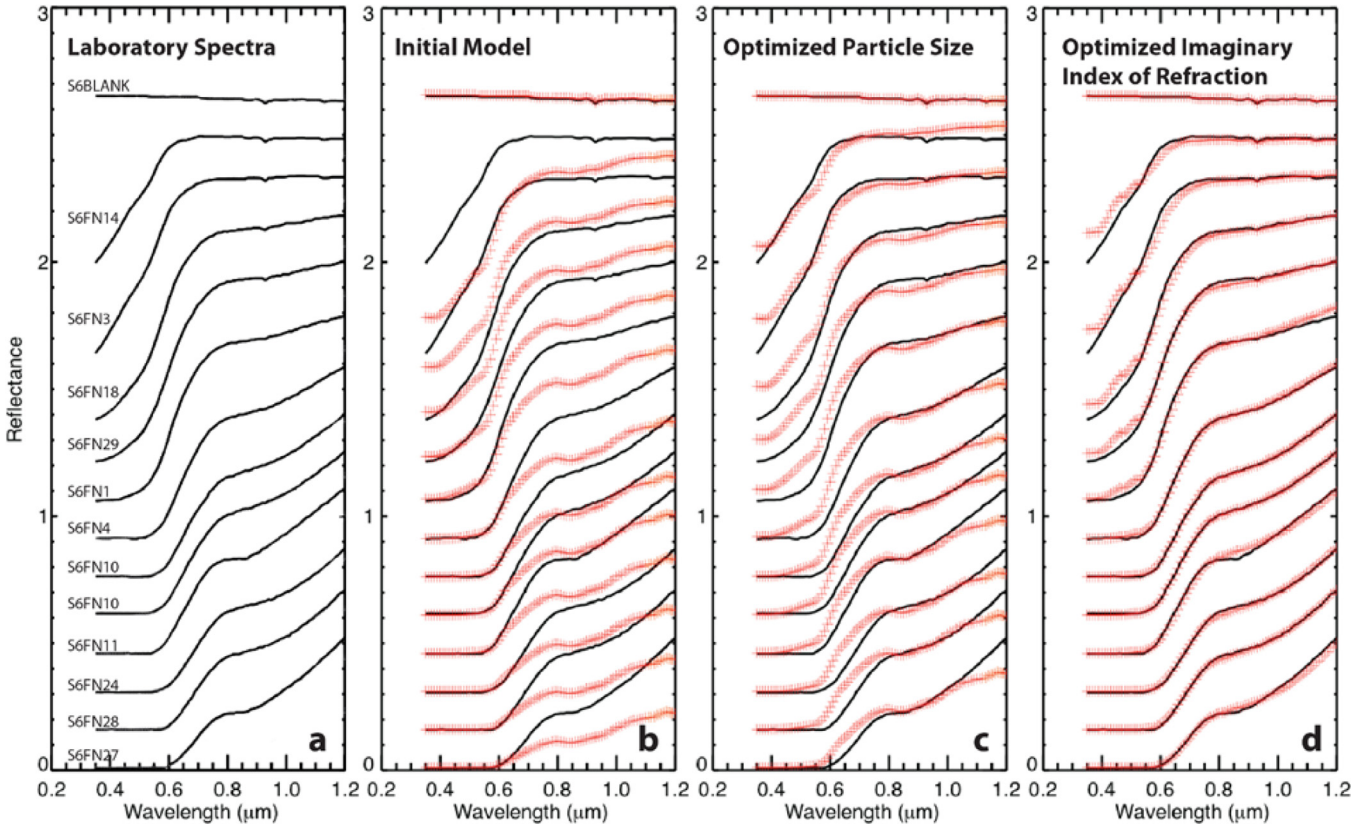

Fig. 1. a) Laboratory spectra of silica gel infused with varying quantities of nanophase hematite (black lines) from Morris et al. (1989) with increasing nanophase hematite from top to bottom (Table 1). The spectra are offset for clarity. b) Red symbols are spectra computed using the Hapke (2001) model and hematite optical constants of Querry (1985). Strong deviations are observed between model and measurements beyond 600 nm where hematite is relatively transparent, and at low ferric oxide abundances. c) Similar to the computation in (b), but this model optimizes the host grain sizes based upon the grain sizes in Fig. 3. d) Similar to the computation in (b), but this model includes modifications to the hematite optical constants to match the Morris et al. (1989) laboratory spectra. (For interpretation of the references to colour in this figure legend, the reader is referred to the web version of this article.)

samples. The radiative transfer technique requires relatively few inputs: the real and imaginary indices of refraction (n and k) of the host and nanophase particles, the grain size of the host particle, and the abundance of nanophase particles. The specific values are as follows: (1) The host particles (the silica gels) are assigned a grain size of 60 μm, which is about the mean sieve size fraction of the Morris et al. (1989) silica gels used in this study. (2) The real index of refraction for the host particles is set at 1.5 for all wavelengths, which is the visible real index of refraction of silica gel (Morris et al., 1989). (3) The imaginary index of refraction of the host particles is computed using Hapke theory (i.e., Hapke, 1993) from the reflectance of the iron-free silica gel sample (i.e., S6BLANK from Table 1). First we converted the S6BLANK reflectance spectrum to a single scattering albedo spectrum by inverting Equation 10.17 of Hapke (1993) and assuming an incidence angle of 0°. The single scattering albedo was converted to the imaginary index of refraction using the Hapke-based method of Lucey (1998). (4) We used Querry's (1985) optical constants of hematite for the real and imaginary index of refraction of the nanophase particles. (5) Ferric oxide abundances are from Morris et al. (1989), which are listed in Table 1. With the necessary variables defined, we tested the radiative transfer model against Morris's et al. (1989) laboratory spectra (Fig. 1a).

3. Results and model improvements

Fig. 1b shows our radiative transfer model spectra plotted with the laboratory spectra of Morris et al. (1989). While the general model spectral shapes are grossly similar to the laboratory spectral shapes, the reflectance values and detailed spectral shapes are different. Fig. 2a plots the single scattering albedo against the ferric oxide abundance at various wavelengths. At shorter wavelengths, which is where the nanophase hematite particles are more absorbing, the model spectra match the abundance and reflectance trends of laboratory spectra, but at longer, more transparent wavelengths, the model significantly underestimates the reflectance at all ferric oxide abundances.

We explored two modifications to the model to improve the fits to the data: (1) altering the host grain size and (2) altering the values of the optical constants of hematite, per the suggestion of Morris and Lauer (1990). In Hapke's radiative transfer model, the physical particle size of the host is only an approximation of the mean optical path of light through particles (Hapke, 1993; 2001). Hapke (1993) recommends wavelength-independent scaling factors to convert the physical particle size of the host to effective particle size. In the models shown in Fig. 1b, the effective particle size was set equal to the physical particle size. To investigate whether grain size of the host (i.e., silica gel) is a major factor in the discrepancy between the model and laboratory spectra, we found the optimum particle size at each wavelength that would force an optimal fit to the single scattering albedo against the ferric oxide content (Fig. 3). We found that this method reconciled the difference between the model and laboratory spectra at longer wavelengths (Figs. 1c and 2b). However, the physical reasonableness of a possible decrease in effective grain size of the host with increasing wavelength is questionable. This cannot be due to the nanophase hematite as the

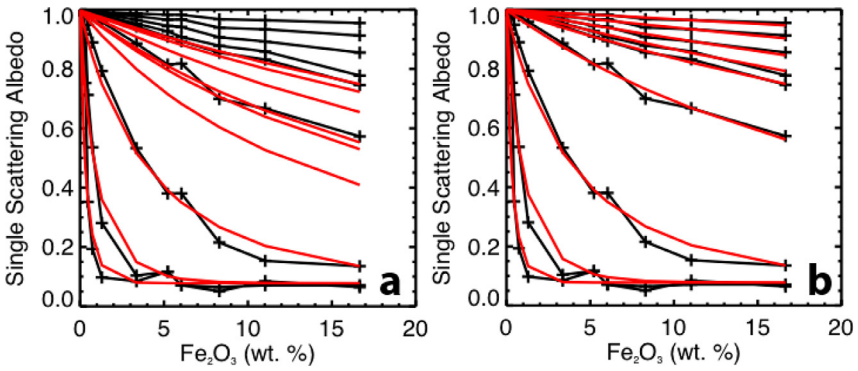

Fig. 2. Black crosses and lines are data from Morris et al. (1989) at 400, 500, 600, 700, 800 900, 1000, 1100 and 1200 nm (bottom to top). a) Red lines are computed from the Hapke (2001) model using a host grain size of 60 μm, the optical constants of Querry (1985), and the ferric oxide abundance provided in Morris et al. (1989). b) The red lines are computed from the Hapke (2001) model with host grain sizes optimized to improve the fits at each wavelength. (For interpretation of the references to colour in this figure legend, the reader is referred to the web version of this article.)

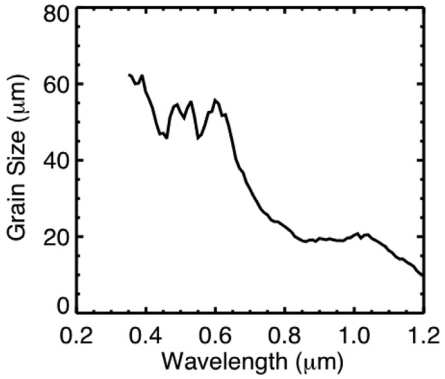

Fig. 3. Host grain sizes optimized to match the ferric oxide data against single scattering albedo at each wavelength.

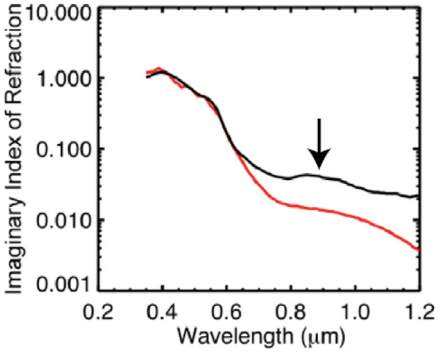

Fig. 4. Imaginary index of refraction of Querry (1985) (black) and the optimized imaginary index of refraction estimated using the Hapke model and data from Morris et al. (1989) (red). The estimated data lack the 860-nm band (black arrow) and are much less absorbing past 600 nm. (For interpretation of the references to colour in this figure legend, the reader is referred to the web version of this article.)

scattering efficiency of subwavelength particles is extremely low and is in fact negligible at all wavelengths (Hapke, 1993; Lucey and Riner, 2011). This includes Rayleigh scattering that, despite its fourth power dependence on wavelength, has very small absolute scattering efficiency and is more effective at shorter, not longer wavelengths. An additional discrepancy is that the 860-nm absorption, easily seen in the spectra of bulk hematite, is present and much stronger than what is observed in the Morris et al. (1989) Type D spectral data (Fig. 1b).

These results show that the spectral effects of the presence of nanophase particles as modeled by Hapke (2001) cannot account for the spectral difference between material containing large bulk particles of hematite and those containing nanophase hematite, including the weakening of the 700 and 860 nm spectral features. This leaves the suggestions of Morris et al. (1989) and Morris and Lauer (1990) that the optical constants of hematite itself differ between bulk and nanophase size fractions. While previous hematite optical constants are not sufficient for this work (i.e., modeling of laboratory and Curiosity spectra), we can estimate them using Hapke's equations (e.g., Hapke, 1993; Lucey, 1998).

To improve the nanophase hematite spectral model, we optimized the hematite optical constants against the Morris et al. (1989) spectral data with a fixed host grain size of 60 μm. There is coupling between the real and imaginary index of refraction in this process (i.e., absorption "leaks" into the real index of refraction), so we set the real index of refraction to be equal to Querry's (1985) real index of refraction of the bulk hematite. Then we used Hapke's (2001) method to iteratively solve for the imaginary index of refraction at each wavelength to minimize the difference between the model and measured reflectance spectra versus ferric oxide abundance. The resulting imaginary index of refraction and that of Querry (1985) are shown in Fig. 4. We observed two prominent differences between the two imaginary index of refraction spectra. First, beyond 600 nm, the imaginary index of refraction is lower in the optimized version than the Querry's (1985) version. This is consistent with the underestimate of reflectance by the Hapke (2001) model using the bulk hematite optical constants. Second, the 860-nm band is absent in the optimized version, again consistent with the failures of the Hapke (2001) model when using bulk hematite optical constants. Unsurprisingly, these new optical constants enable better fits to the laboratory reflectance spectra (Fig. 1d). The individual spectra are not perfect fits because at each wavelength the model fits across all spectra, and the model does not pass through all points.

The new optimized optical constants enable some degree of prediction of ferric oxide abundance from observed spectral data. However, Morris et al. (1989) cautioned that their experimental results suggest an ambiguity between ferric oxide abundance and host particle grain size, which is inherent in the structure of the Hapke model when the host particle is relatively transparent. In the Hapke model, the absorption is almost completely dominated by the product of the absorption coefficient ($\alpha = \frac{4\pi k}{\lambda}$) and the effective host grain size, where the absorption coefficient is a linear function of the mass fraction of the nanophase contaminant. Therefore, nanophase hematite abundance cannot be estimated without an assumption regarding host grain size. However, the measured and modeled nanophase hematite abundance derived by

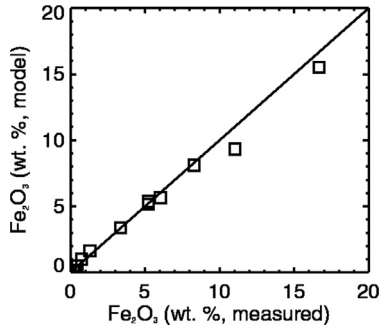

Fig. 5. Correlation of ferric oxide content from fitting the data of Morris et al. (1989) using the Hapke (2001) model, the optical constants of Querry (1985), and the effective host grain size of 25 μm. Almost identical results are found using the new imaginary index estimate and a grain size of 60 μm.

minimizing the differences between measured and model spectra are linearly correlated over a wide range of ferric oxide contents. Using the Querry (1985) optical constants we found that the effective host grain size is 25 μm to optimize the 1:1 correlation between model and measured ferric oxide abundances (Fig. 5). Using our optimized imaginary index of refraction, we observe the same 1:1 result, using a 60 μm host grain size. In comparing the measured and model nanophase hematite abundances, we find that the largest uncertainty is 2 wt%, but the uncertainty decreases at smaller abundances of nanophase hematite.

4. Application to ChemCam passive spectral reflectance data

Having demonstrated that we can confidently estimate the optical constants of hematite and apply them to visible to near-infrared spectra of nanophase hematite-bearing materials, we applied the radiative transfer model with our optimized nanophase hematite optical constants to passive bidirectional reflectance spectral data measured by the Chemistry and Camera (ChemCam) instrument on the Mars Science Laboratory rover, Curiosity. Operated without its laser, the Laser-Induced Breakdown Spectrometer (LIBS) portion of ChemCam can collect spectral relative reflectance data with its three dispersive spectrometers in the ultraviolet (240–342 nm), blue-violet (382–469 nm), and the visible and near infrared (474–906 nm) (Johnson et al., 2015; Maurice et al., 2012). These spectrometers have a spectral resolution of < 1 nm and a spatial resolution of 0.65 mrad. Johnson et al. (2015) obtained, calibrated, and presented reflectance spectra from ChemCam from the first 360 sols of the Curiosity mission for spectra in the 400–840 nm region.

With over 2000 reflectance spectra collected, Johnson et al. (2015) used several spectral parameters, such as band ratios, band depths, and spectral slopes to identify the main end-member spectra. In their analysis, they recognized six classes, *Veins, Raised ridges, Dark rocks, Red rocks, Exposed surfaces,* and *Bradbury landing zone* (Fig. 6). *Exposed surfaces* represent areas that were brushed by the Dust Removal Tool or fractured surfaces due to the rover wheels. The *Dark rocks* exhibit low relative reflectance and an enhanced near-infrared slope. The *Bradbury* spectra originate from areas within the immediate landing zone from Sols 1–20. The *Ridges* spectra come from MgO-bearing raised ridge surfaces. *Red* spectra are from dusty surfaces, which display relatively high reflectances. *Veins* spectra are from calcium sulfate-bearing veins.

We modeled the six main end-member spectra with the Hapke (2001) model. In this analysis we assume the host particles are 6 μm in diameter (Poulet et al., 2007). We used a spectrally neutral host reflectance throughout the visible and near infrared based on the lowest reflectance that allowed a consistent fit to each of the passive reflectance observations with the exception of the Veins class (Table 2), a constant real index of refraction of 1.4, and a density of 3.0 g/cm^3, the average density of silicates. For the Veins class, we used the optical constants of gypsum (i.e., Roush et al., (2007) as the host reflectance because Nachon et al. (2014) found that the *Veins* class to be dominantly gypsum ($CaSO_4{\cdot}2H_2O$) and bassanite ($CaSO_4{\cdot}0{\cdot}5H_2O$). The incidence and emission angles for each spectral observation are listed in Table 2. However, these angles are approximations because they do not account for local incidence and emission angles due to the complex geometry of the target surfaces. To analyze the data we produced a spectral library consisting of thousands of model spectra with varying abundances of nanophase hematite within a transparent host particle from 0–5 wt% at intervals of 0.001 wt%. We found the best-fit model spectrum to a representative end-member passive spectrum by subtracting the representative passive spectrum by each model spectrum in our spectral library and calculating the root-mean-square (RMS). The model spectrum with the smallest RMS is the best-fit model spectrum. Additionally, the model spectra are allowed to additively displace towards higher or lower reflectance due to the uncertainty in the local incidence and emission angles.

Fig. 6 shows the best-fit model spectrum to each of the six end-member spectra. In general, the shape of the model spectra matched the shape of the passive reflectance spectra. The most consistent fits are the *Bradbury* and the *Dark* classes. The *Ridge* and *Red* classes are consistent, except in the 0.4–0.5 μm portion of the spectra where the model spectra do not flatten out as quickly as the observed spectra. However, this region is affected by a lack of data in the 468–474 nm region resulting from a gap in wavelength coverage between two of the ChemCam detectors. The model spectrum of the *Exposed* class spectrum changes slope at a longer wavelength (0.6 μm) than the observed *Exposed* class spectrum (0.5 μm). The *Veins* class observed spectrum and the model spectrum show similar curvature, but the details of the spectral shape do not match.

The relative model nanophase hematite abundances are within our expectations. For example, the *Dark* and *Exposed* classes lack significant aeolian dust (Johnson et al., 2015), which suggests the abundances should be low. Our model shows that these two classes have less than ≤ 1.0 wt% nanophase hematite. In addition, the *Veins* class contains 0.4 wt% nanophase hematite, which

Table 2
Metadata of Curiosity's passive spectral reflectance data of six representative samples.

Rock Class	Representative	Incidence [°]	Emission [°]	Phase [°]	Host Reflectance	np Hematite Abund. [wt%]
Bradbury	Coronation	18.1	42.4	25.1	20%	0.1
Red	Rifle	15.9	67.6	54.5	50%	3.6
Veins	Rapitan	15.0	43.6	33.4	Gypsum OC*	0.4
Exposed	Werneck1Brush	19.6	37.7	55.3	40%	0.4
Ridges	McGrath4	23.3	32.0	55.1	40%	0.8
Dark	Ashuanipi	13.3	60.2	52.3	20%	0.1

*OC - Optical Constants based on Roush et al. (2007).

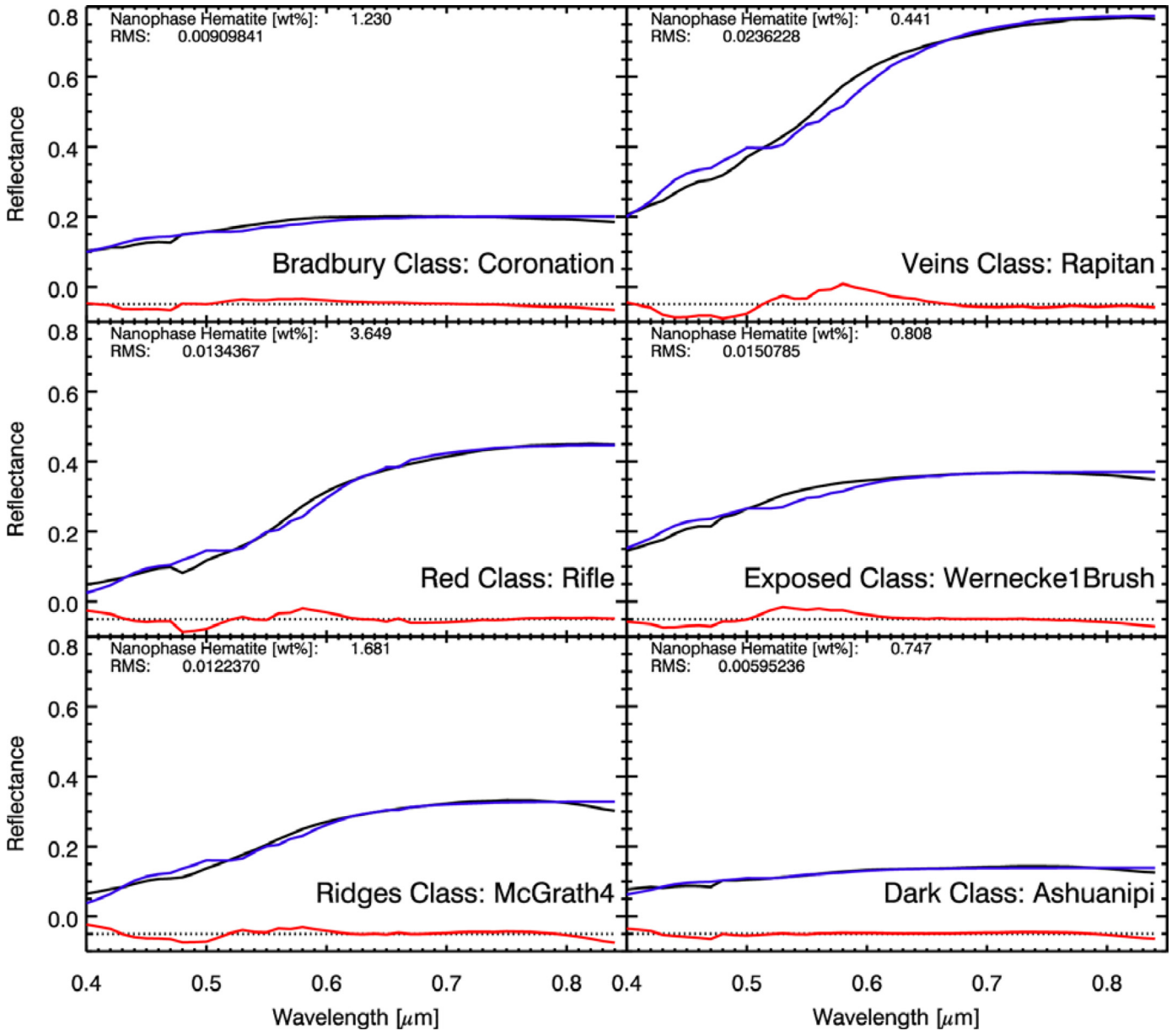

Fig. 6. A comparison between the passive reflectance spectra from ChemCam (black) and the best-fit model spectra (blue) based upon the optimized imaginary index of refraction optical constants and Hapke (2001). We also included the RMS, the model abundance, and residuals (red) for each spectrum. (For interpretation of the references to colour in this figure legend, the reader is referred to the web version of this article.)

may be due to removal of the dust by the LIBS analysis prior to the passive spectral measurements (Nachon et al. 2014). On the other hand, the *Bradbury, Red,* and *Ridge* class contains > 1.0 wt% nanophase hematite, which is expected at least for the *Red* class, which contains > 100 μm layer dust, in contrast to the *Bradbury* class, which is predicted to have a < 50 μm layer of dust (Johnson et al., 2015).

5. Conclusion

In this work, we developed a radiative transfer model to model the laboratory spectra of nanophase hematite (< 10 nm). Unmodified, the Hapke (2001) nanophase model used with the Querry (1985) bulk hematite optical constants deviates significantly from the laboratory spectral measurements of Morris et al. (1989) at longer wavelengths where hematite is relatively non-absorbing, an issue observed in previous works (e.g., Steyer, 1974; Marra et al., 2011). While shortcomings of the model or our assumptions are certainly possibilities, we found that modification of the imaginary index of refraction of hematite, which is needed given the nanophase nature of the particles in the Morris et al. (1989) samples, enables close reproduction of the Morris et al. (1989) spectra. Our model spectra support the hypothesis presented by Morris et al. (1989) that spectral differences arise due to the dominant crystalline structure of bulk and nanophase hematite. Finally, the correlation between ferric oxide reflectance and grain size is sufficiently linear to enable prediction of ferric oxide content from spectra, but there is an inherent ambiguity between host particle grain size and ferric oxide content, so the quality of the prediction is limited by uncertainties with respect to the grain size. We applied the new optical constants of nanophase hematite to the passive spectral reflectance data from ChemCam. We found that applications of these new optical constants are able to match the general shape of the observed

spectra of six end-members. We found that the estimated abundances of nanophase hematite were higher in dusty areas, and generally found the nanophase contents to be small, no more than 4 wt%.

Acknowledgements

We would like to thank two anonymous reviewers for their critical reviews. This work was supported in part by a NASA Planetary Geology and Geophysics grant (NNX 1408 G) to T. D. Glotch. NASA was not involved in the study design, the data collection, analysis, and interpretation, in the writing of the report, or in the decision to submit the article for publication. SOEST publication #10226 and HIGP publication #2261.

References

Bedidi, A., Cervelle, B., 1993. Light scattering by spherical particles with hematite and goethite-like optical properties: effect on water impregnation. J. Geophys. Res. 98 (B7), 11941–11952. doi:10.1029/93JB00188.

Bell, J.F., et al., 2004. Pancam multispectral imaging results from the opportunity rover at Meridiani Planum. Science 306, 1703–1709.

Gillespie, J.B., Lindberg, J.D., 1992. Ultraviolet and visible imaginary refractive index of strongly absorbing atmospheric particulate matter. Appl. Opt. 31 (12), 2112–2115.

Glotch, T.D., Christensen, P.R., Sharp, T.G., 2006. Fresnel modeling of hematite crystal surfaces and application to martian hematite spherules. Icarus 181, 408–418. doi:10.1016/j.icarus.2005.11.020.

Hapke, B., 1993. Theory of Reflectance and Emittance Spectroscopy. Cambridge University Press, New York, p. 469.

Hapke, B., 2001. Space weathering from Mercury to the asteroid belt. J. Geophys. Res. 106 (E5) 10,039-010,073, doi:10.1029/2000JE001338.

Johnson, J.R., et al., 2015. ChemCam passive reflectance spectroscopy of surface materials at the Curiosity landing site, Mars. Icarus 249 (First Year of MSL), 74–92. doi:10.1016/j.icarus.2014.02.028.

Keller, L.P., McKay, D.S., 1997. The nature and origin of rims on lunar soil grains. Geochim. et Cosmochim. Acta 61 (11), 2331–2341. doi:10.1016/S0016-7037(97)00085-9.

Kerker, M., Scheiner, P., Cooke, D.D., Kratohvil, J.P., 1979. Absorption index and color of colloidal hematite. J. Coll. Interf. Sci. 71 (1), 176–187.

Lucey, P.G., 1998. Model near-infrared optical constants of olivine and pyroxene as a function of iron content. J. Geophys. Res 103 (E1), 1703–1713. doi:10.1029/97JE03145.

Lucey, P.G., Noble, S.K., 2008. Experimental test of a radiative transfer model of the optical effects of space weathering. Icarus 197 (1), 348–353. doi:10.1016/j.icarus.2008.05.008.

Lucey, P.G., Riner, M.A., 2011. The optical effects of small iron particles that darken but do not redden: evidence of intense space weathering on Mercury. Icarus 212 (2), 451–462. doi:10.1016/j.icarus.2011.01.022.

Marra, A.C., Blanco, A., Fonti, S., Jurewicz, A., Orofino, V., 2005. Fine hematite particles of Martian interest: absorption spectra and optical constants. J. Phys. 6 (6), 132–138. doi:10.1088/1742-6596/6/1/013.

Marra, A.C., Lane, M.D., Orofino, V., Blanco, A., Fonti, S., 2011. Midinfrared spectra and optical constants of bulk hematite: comparisons with particulate hematite spectra. Icarus 211, 839–848. doi:10.1016/j.icarus/2010.09.021.

Maurice, S., et al., 2012. The ChemCam instrument suite on the Mars science laboratory (MSL) rover: science objectives and mast unit description. Space Sci. Rev 170 (1), 95–166. doi:10.1007/s11214-012-9912-2.

McCord, T.B., Huguenin, R.L., Johnson, G.L., 1977. Photometric imaging of Mars during the 1973 opposition. Icarus 31 (3), 293–314. doi:10.1016/0019-1035(77)90024-0.

Morris, R.V., 1976. Surface exposure indices of lunar soils: a comparative FMR study. In: Proc. Lunar Sci. Conf. 7th, 1, pp. 315–335.

Morris, R.V., 1978. The surface exposure (maturity) of lunar soils: Some concepts and Is/FeO compilation. In: Proc. Lunar Planet. Sci. Conf. 9th, 2, pp. 2287–2297.

Morris, R.V., Agresti, D.G., Lauer, H.V., Newcomb, J.A., Shelfer, T.D., Murali, A.V., 1989. Evidence for pigmentary hematite on Mars based on optical, magnetic and mossbauer studies of superparamagnetic (nanocrystalline) hematite. J. Geophys. Res 94 (B3), 2760–2778.

Morris, R.V., et al., 2006. Mössbauer mineralogy of rock, soil, and dust at Gusev crater, Mars: spirit's journey thorugh weakly altered olivine basalt on the plains and pervasively altered basalt in the Columbia Hills. J. Geophys. Res. 111, E02S13. doi:10.1029/2005JE002584.

Morris, R.V., Lauer, H.V., 1990. Matrix effects for reflectivity spectra of dispersed nanophase (superparamagnetic) hematite with application to Martian spectral data. J. Geophys. Res. 95 (B4), 5101–5109. doi:10.1029/JB095iB04p05101.

Nachon, M., et al., 2014. Calcium sulfate veins characterized by ChemCam/Curiosity at Gale Crater, Mars. J. Geophys. Res. 119, 1991–2016. doi:10.1002/2013JE004588.

Noble, S.K., Pieters, C.M., Keller, L.P., 2007. An experimental approach to understanding the optical effects of space weathering. Icarus 192 (2), 629–642. doi:10.1016/j.icarus.2007.07.021.

Onari, S., Arai, T., Kudo, K., 1977. Infrared lattice vibrations and dielectric dispersion in α-Fe_2O_3. Phys. Rev. B 16 (4), 1717–1721.

Popova, S., Tolstykh, T., Ivlev, L., 1973. Optical-Constants of Fe_2O_3 in infrared specral region. Optika Spektrosc 35, 954–955.

Poulet, F., Gomez, C., Bibring, J.-P., Langevin, Y., Gondet, B., Pinet, P., Belluci, G., Mustard, J., 2007. Martian surface mineralogy from Observatoire pour la Minéralogie, l'eau, les Glaces et l'Activité on board the Mars Express spacecraft (OMEGA/MEx): global mineral maps. J. Geophys. Res. 112, E08S02. doi:10.1029/2006JE002840.

Querry, M.R., 1985. Optical Constants. Missouri University, Kansas\sCity, Kansas City.

Roush, T.L., Esposito, F., Rossman, G.R., Colangeli, L., 2007. Estimate optical constants of gypsum in the regions of weak absorptions: Applications of scattering theories and comparisons to independent measurements. J. Geophys. Res 112, E10003. doi:10.1029/2007JE002920.

Singer, R.B., McCord, T.B., Clark, R.N., Adams, J.B., Huguenin, R.L., 1979. Mars surface composition from reflectance spectroscopy: a summary. J. Geophys. Res. 84, 8415–8426.

Steyer, T.R., 1974. Infrared Optical Properties of Some Solids of Possible Interest in Astronomy and Atmospheric Physics. The University of Arizona, Tucson, AZ., p. 157.

Yen, A., et al., 2005. An integrated view of the chemistry and mineralogy of martian soils. Nature 436, 49–54. doi:10.1038/nature03637.